CHAPTER 2

7-Azaindole with One to Five Water Clusters ($7AI(H_2O)_{1–5}$)

2.1 Introduction

Proton transfer plays crucial roles in a variety of chemical and biological reactions [1–5] such as enol–keto tautomerization [6], proton transport via membrane-spanning proteins [7, 8], and proton relay system in enzymes [8]. The phototropic tautomerism of DNA base pairs, which has attracted much interest due to its relation to UV-induced gene mutation, has the excited-state proton-transfer (ESPT) phenomena as the primary molecular step [60]. Generally, it is specially challenging to monitor ESPT in natural nucleobases and nucleobase pairs due to their conformational and spectroscopic complexity [61-62]. In this context, 7-azaindole (7AI, Figure 2.1), a spectroscopically simpler prototype for purine nucleobases [60], emerges as a good alternative for basic sciences research. It has also been claimed that 7AI can advantageously replace tryptophan, customarily considered as the standard optical probe of protein structure and dynamics [63-65]. As a result, ESPT in 7AI monomer within small molecular clusters and in bulk solvents has been extensively studied by experimentalists and theorists [25-52].

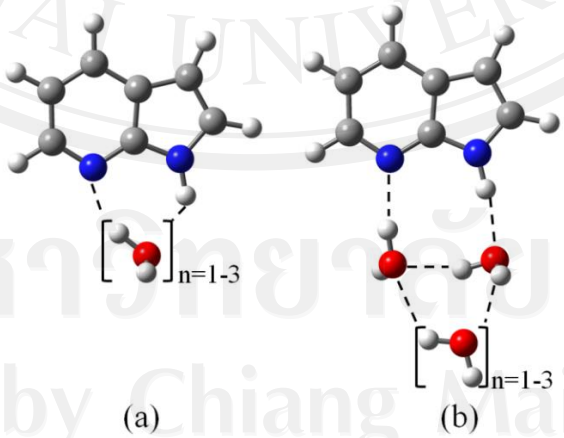

Figure 2.1 Structure of 7AI with water molecules showing (a) first hydration shell and (b) first and second hydration shells

It is well known that the isolated 7AI molecule cannot undergo ESPT without assistance of solvent molecules [66]. With cooperation of a single water molecule (Figure 2.1), the energy barrier required for tautomerization of 7AI is considerably reduced in the ground and excited states as reported by Chaban and Gordon [39, 67]. The barrier heights for ESPT are even lower within clusters with two waters [41].

When 7AI-water clusters are excited into the S_1 band origin, ESPT occurs slow [68-70]. For 7AI$(H_2O)_3$, for instance, while the excited-state lifetime (an upper bound to the ESPT time) is more than 10 ns at 0_0^0, it is reduced to only 15 ps upon an energy excess of 300 cm^{-1} [71]. Ab initio molecular dynamics (AIMD) simulations on 7AI$(H_2O)_{1,2}$ reported by Kina et al. [51] showed that the excited-state transfer occurs about 50 fs after photoexcitation about 12,000 cm^{-1} energy excess.

7AI-water clusters with more than three waters have received less attention because it is believed that such large clusters cannot be directly involved in the tautomerization. Moreover, these clusters are difficult to be spectroscopically assigned due to the complexity of their electronic [62] and vibrational [61] structures. 7AI with four waters was studied by Folmer et al. [43] using ultrafast pump–probe spectroscopy combined with theoretical calculations. Their results revealed that the proton-transfer rate increases compared to that of 7AI with two and three waters. Their deuteration studies provided proof for the occurrence of proton transfer (PT), although it was not conclusively confirmed that the proton transfer resulted in a complete tautomerization of the 7AI monomer. For even bigger clusters of 7AI with five waters, there are no experimental investigations available; only a theoretical study was reported on the second hydration shell effect [72].

Recently, Yu et al. [73] reported a theoretical investigation of ESPT on clusters of 7AI with three water molecules by using time-dependent density functional theory (TDDFT), complete active space perturbation theory to the second order (CASPT2) and coupled cluster with approximated doubles (CC2). Their static calculations on the first excited state suggested the possibility of hydrogen bond rearrangement (HBR) of water molecules from a bridged-planar isomer to a cyclic-nonplanar isomer, followed by triple proton transfer. They also found out that triple PT in the cyclic-nonplanar isomer is energetically more favorable than the quadruple PT in the bridged-planar isomer. It was concluded that all proton-transfer processes follow a synchronous mechanism. (In their

paper, they call ‘‘concerted’’ what we call ‘‘synchronous’’ in the present work. This classification is discussed below in Excited-state dynamics simulations.) Furthermore, the barrier for HBR was found to be less than 1 kcal.mol^{-1}, consistent with the missing vibronic bands in the resonance-enhanced multiphoton ionization (REMPI) spectra for 7AI$(H_2O)_3$ [71]. Another recent theoretical study using on-the-fly dynamics simulations was carried out by our group for the multiple proton transfer in the first excited state of 7AI in the clusters of methanol [36] and mixed methanol–water [37] employing the algebraic diagrammatic construction to the second-order (ADC(2)) scheme. The results showed that the PT is completed in the 100 fs timescale and tends to be slower in methanol than in water because of the lower polarity of the former.

Based on all those previous studies mentioned above, especially the isomerization of 7AI$(H_2O)_3$ by Yu et al. [73], it occurred to us that the ab initio molecular dynamics simulations of 7AI$(H_2O)_n$ with different isomers and different cluster sizes would be a very interesting way of testing the reaction paths for ultrafast ESPT, specially the role of the second hydration shell. Therefore, the purpose of this work is to carry out a systematic study of ESPT dynamics in 7AI$(H_2O)_{1–5}$ clusters. The main goals are to determine the dynamic behavior of different water clusters around 7AI, the dependence of the ultra-fast excited-state tautomerization probability with the cluster size, the effect of hydrogen bond arrangement for clusters with the same number of water but different conformations, and the role played by water in different cluster sizes.

2.2 Computational details

2.2.1 Ground-state calculations

Ground-state geometries of 7AI$(H_2O)_{n=1–5}$ clusters in the gas phase were optimized with the second-order Møller–Plesset Perturbation Theory (MP2) with the resolution of-the-identity (RI) approximation for the electron repulsion integrals [57-58]. The split valence polarized (SVP) [74] basis set was assigned to heavy atoms and hydrogen atoms involved in the hydrogen-bonded network, whereas the split-valence (SV(P)) [74] basis set was assigned to the remaining hydrogen atoms in the clusters, as implemented in the program package TURBOMOLE 5.10 [75]. The performance of this basis set was tested with comparisons to results computed with the TZVPP [76] basis set. For 7AI$(H_2O)_2$, two isomers were investigated. For 7AI$(H_2O)_3$, three different isomers were determined based on previous results by Pino et al. [71] and Yu et al. [73]. For 7AI$(H_2O)_4$, a cyclic isomer

with two circuits was chosen, corresponding to an isomer reported by Folmer et al. [43] and Casadesus et al. [77]. Similarly, for $7AI(H_2O)_5$, the cyclic cluster with two circuits was selected. This isomer has also been previously reported by Fernandez-Ramos et al. [72]. All optimized structures were confirmed to be minima on the ground-state surface by normal-mode analysis.

2.2.2 Excited-state dynamics simulations

On-the-fly Born–Oppenheimer dynamics simulations on the first excited-state (S_1) potential energy surface were carried out for the $7AI(H_2O)_{1–5}$ clusters at RI-ADC(2)/SVP-SV(P) level. The ADC(2) method, originally derived using diagrammatic perturbation theory [78-79], can be expressed by the symmetric Jacobian $A^{ADC(2)} = \frac{1}{2}(A^{CIS(D\infty)} + A^{CIS(D\infty)\dagger})$, where $A^{CIS(D\infty)}$ is the Jacobian of the CIS(D∞) coupled-cluster approximation [58]. The ADC(2) excited-state energies correspond to the eigenvalues of the Jacobian, while the ground-state energy is given by the MP2 method. ADC(2) has a computational cost similar to that of coupled cluster to approximated second order (CC2), with comparable accuracy [80]. ADC(2), however, possesses the distinct advantage over CC2 of deriving from a Hermitian eigenvalue problem. This increases its numerical stability in the case of quasidegenerate excited states and reduces the computational effort required for the computation of molecular properties and gradients. The current implementation of ADC(2) is explained in Ref. [81], and the computation of its analytical gradients is explained in Ref. [57]. Initial conditions were generated using a harmonic oscillator Wigner distribution for each vibrational normal mode, as implemented in the NEWTON-X program package [82-83] interfaced with the TURBOMOLE program. Excitation into the entire S_1 band was allowed to provide enough energy to activate ultrafast processes. Dynamics simulations in the first excited state were carried out with the NEWTON-X program in microcanonical ensembles using Born–Oppenheimer energies and gradients provided by RI-ADC(2) in the TURBOMOLE program. The nuclear motion of all atoms in the clusters was treated classically and computed by numerical integration of Newton's equation by the Velocity Verlet algorithm [84-85]. Fifty trajectories for each cluster and each different isomer—totalizing 400 trajectories—were simulated with a time step of 1 fs. Trajectories were propagated for 300 fs, enough to cover the pre- and post-PT regimes. A subset of five trajectories for one of the three $7AI(H_2O)_3$ isomers was extended up to 1,000 fs to check the possibility of hydrogen bond

rearrangement. Furthermore, a statistical analysis was carried out to deliver detailed geometric and energetic properties, which were used to describe the time evolution of the reactions along the hydrogen-bonded network.

Neither tunneling nor nonadiabatic effects were considered in this work. Tunneling could be discarded as our focus was on the description of the ultrafast proton transfer (sub-picosecond scale). Based on our previous investigations of these systems [36-37], we did not expect occurrence of surface crossings that would demand a nonadiabatic treatment. This was confirmed by the dynamics results, which showed that the character of the S_1 state was always a ππ* excitation. The ππ* character of the S_1 state implies that a proton—rather than a hydrogen atom—is transferred. For having a hydrogen transfer, the character of the S_1 state would be πσ* (see, for instance, Ref. [22]). We did not observe diabatic changes between ππ* and πσ* characters along the dynamics. The separation between these states is illustrated for one single trajectory of $7AI(H_2O)_3$ in Figure 2.2.

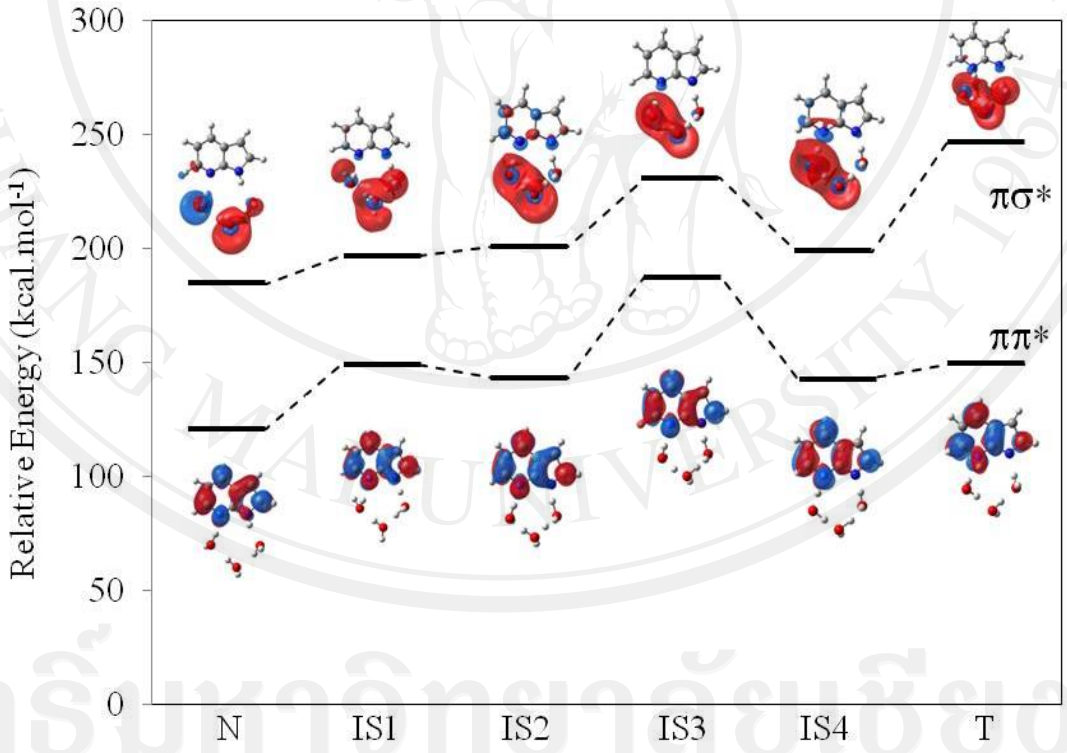

Figure 2.2 Relative single-point energies at RI-ADC(2)/SVP-SV(P) of first excited-states (ππ* and πσ*) of a selected trajectory for the $7AI(H_2O)_3$-bridged-planar cluster

2.3 Results and discussion

2.3.1 Ground-state structures

The ground-state geometries of all clusters were optimized at RI-ADC(2)/SVP-SV(P) level. Figure 2.3 shows the ground-state geometries of all three investigated isomers of 7AI$(H_2O)_3$. Intermolecular hydrogen bonds of 7AI with water and between water molecules are indicated by dashed lines. The energies of these three isomers are less than 2.4 kcal.mol^{-1} apart (Table 2.1), in good agreement with results reported by Yu et al. [73] and Sakota et al. [47, 71]. The cyclic-nonplanar (Figure 2.3b) is the lowest energy structure, followed by the bridged-planar (Figure 2.3a) and then by the bicyclic-nonplanar isomer (Figure 2.3c). Dynamics starting from the cyclic-nonplanar isomer was specially set to test the HBR proposed by Yu et al. [73].

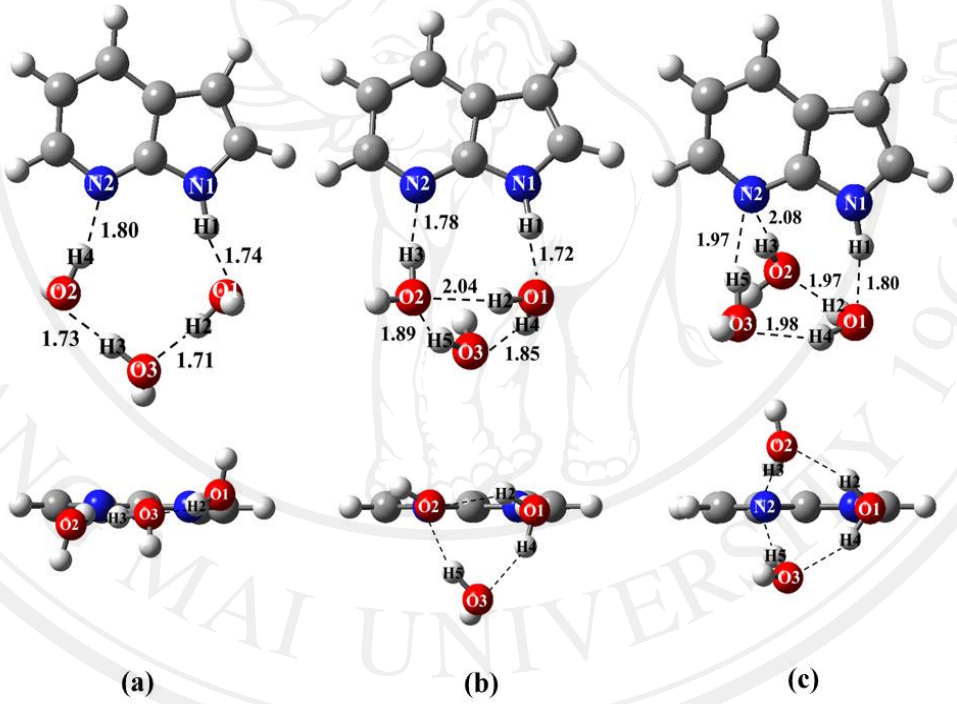

Figure 2.3 Three different isomers of 7AI$(H_2O)_3$ optimized at RI-ADC(2)/SVP-SV(P) level: (a) bridged-planar, (b) cyclic-nonplanar and (c) bicyclic-nonplanar. First row is top view and second row is side view

The ground-state optimized geometry of 7AI$(H_2O)_4$ is shown in Figure 2.4a. There are other possible ground-state structures, but only one candidate to exhibit two circuits for the proton transfer was found. The first circuit includes the two nearest waters (first shell), while the second circuit includes all four waters. This structure, which can

Table 2.1 Relative energy of three different ground-state isomers of 7AI$(H_2O)_3$ optimized at RI-ADC(2)/SVP-SV(P) level: (a) bridged-planar, (b) cyclic-nonplanar (2+1), and (c) bicyclic-nonplanar

Isomer	**Energy (kcal.mol^{-1})**		
	ADC(2) Present result	**MP2/cc-pVDZ (B3LYP/cc-pVDZ) by Yu et al. (2012)**	**CC2/cc-pVDZ (B3LYP/cc-pVDZ) by Pino et al. (2011)**
Bridged-planar	0.00	0.00 (0.00)	0.00 (0.00)
Cyclic-nonplanar	-1.57	-0.93 (-0.86)	-
Bicyclic-nonplanar	0.82	0.14 (1.90)	-1.33 (-2.91)

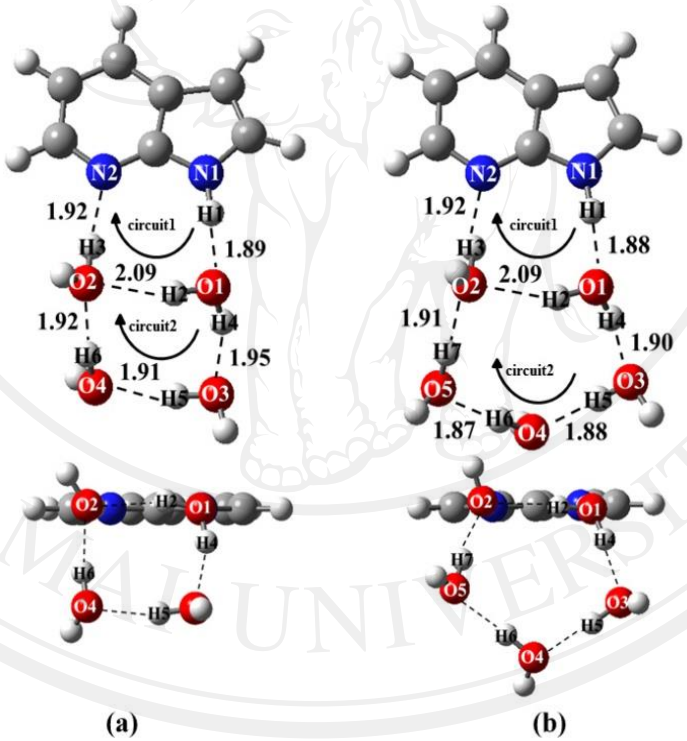

Figure 2.4 Ground-state geometries of (a) 7AI$(H_2O)_4$ and (b) 7AI$(H_2O)_5$ optimized at RI-ADC(2)/SVP-SV(P) level

be viewed as 7AI$(H_2O)_{2+2}$, is similar to the B3LYP results reported by Casadesus et al. [77]. Based on Hartree–Fock level optimizations, Folmer et al. [43] also reported a 7AI$(H_2O)_{2+2}$ structure. The orientation of the first water in their work, however, is somewhat different from our result and from that of Ref. [77].

The ground-state optimized structure of 7AI$(H_2O)_5$ as a cyclic 7AI$(H_2O)_2$ with three additional water molecules is illustrated in Figure 2.4b. This structure, also previously reported by Fernandez-Ramos et al. [72], was chosen to investigate the effect of the second hydration shell. Like the 7AI$(H_2O)_4$ cluster, it has two circuits with a well formed hydrogen-bonded network of water molecules. Proton transfer might occur either through circuit1, involving two waters, or through circuit2, involving all five waters.

The ground-state geometries of 7AI$(H_2O)_1$ and two isomers with two waters, 7AI$(H_2O)_{1+1}$ and 7AI$(H_2O)_2$, were also computed and further employed for initiating dynamics simulation. Their optimized geometries are shown in Figure 2.5.

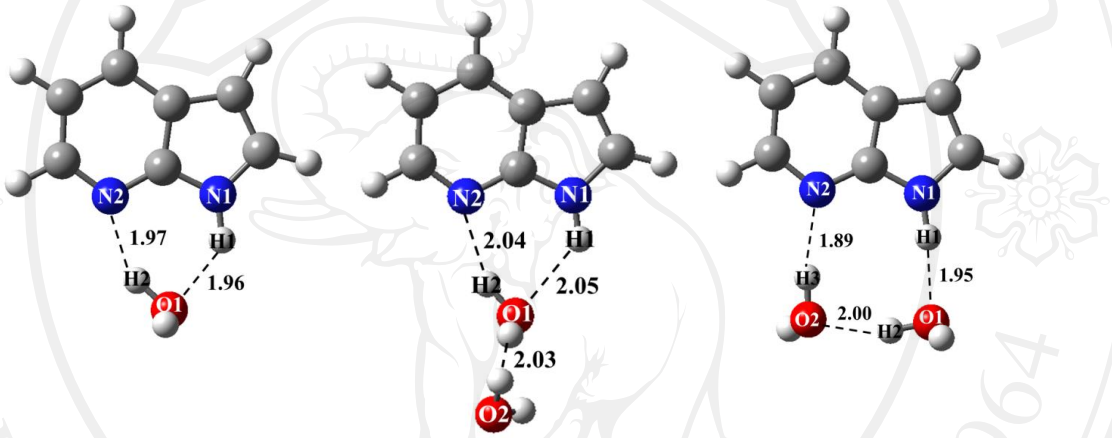

Figure 2.5 Ground-state structures of 7AI$(H_2O)_1$, 7AI$(H_2O)_{1+1}$, and 7AI$(H_2O)_2$ optimized at ADC(2)/SVP-SV(P)

2.3.2 Excited-state dynamics simulations

On-the-fly dynamics simulations in the S_1 excited state were carried out for all 7AI$(H_2O)_{1–5}$ clusters described above. The simulated trajectories were sorted into two types of reaction: (1) ‘‘ESPT’’ when 7AI tautomerization is complete within the simulation time (300 fs); and (2) ‘‘NT’’ (for ‘‘No tautomerization’’) when tautomerization does not take place within the simulation time. The number of trajectories in each type of reaction, the probability of tautomerization (ratio between the number of ESPT trajectories and the total number of trajectories), and the average time of PT for each cluster are summarized in Table 2.2. The error bars for the statistical uncertainty are given for 90 % confidence interval. The PT distance, averaged over all ESPT trajectories, is also given in Table 2.2. The results are discussed in the next sections.

Table 2.2 Summary of the excited-state dynamics performed at RI-ADC(2)/SVP-SV(P): number of trajectories showing 7AI tautomerization (ESPT) or no tautomerization (NT), tautomerization probability, and average time to complete the proton transfers. Average distances at the proton-transfer time are given in parenthesis (Å)

Complex	Reaction		Tautom.	Time (fs)			
	ESPT	NT	Probability	PT1	PT2	PT3	PT4
$7AI(H_2O)_1$	12	38	0.24 ± 0.10	48 (1.34)	59 (1.39)		
$7AI(H_2O)_{1+1}$	18	32	0.36 ± 0.11	91 (1.39)	96 (1.37)		
$7AI(H_2O)_2$	20	30	0.40 ± 0.11	69 (1.28)	70 (1.28)	78 (1.31)	
$7AI(H_2O)_3$ bridged-planar	3 1[a]	46	0.06 ± 0.06	69 (1.29)	73 (1.30)	79 (1.31)	90 (1.33)
$7AI(H_2O)_3$ cyclic-nonplanar	19	31	0.38 ± 0.11	77 (1.30)	91 (1.34)	99 (1.35)	
$7AI(H_2O)_3$ bicyclic-nonplanar	30	20	0.60 ± 0.10	70 (1.27)	105 (1.30)	115 (1.34)	
$7AI(H_2O)_4$	40 1[b]	9	0.82 ± 0.08	74 (1.27)	83 (1.31)	95 (1.29)	
$7AI(H_2O)_5$	38 3[c]	9	0.82 ± 0.08	74 (1.27)	85 (1.33)	111 (1.27)	

[a] HBR trajectory was included neither in the probability nor in the PT time analysis.

[b] Quintuple ESPT trajectory and [c] Sextuple ESPT trajectories were included in the probability analysis, but not in the PT time analysis.

The PT time is defined as the time when the breaking bond length averaged over all ESPT trajectories intersects the average forming bond length. This is the same definition that we have used in our previous investigations [36, 86-88]. The PT mechanism can be assigned as either synchronous, concerted or sequential depending on the time lag between two consecutive PTs [89]. If the delay time is shorter than about

10–15 fs, which corresponds to a vibrational period of N–H and O–H stretching modes, the PT processes are synchronous. Otherwise, they are either concerted (a single kinetic step) or sequential (two distinct kinetic steps via a stable intermediate). It will be concerted if the PTs take place within the time of few N–H stretching modes (roughly, less than 100 fs), and it will be sequential if there is enough time to form a stable intermediate (>100 fs). Average time lags between each PT used to classify the mechanisms are listed in Table 2.3.

Table 2.3 Time lag of the excited-state dynamics simulation

Complex	**Time (fs)**						
	PT1	**Time lag**	**PT2**	**Time lag**	**PT3**	**Time lag**	**PT4**
7AI(H_2O)$_1$	48	*10*	59				
7AI(H_2O)$_{1+1}$	91	*5*	96				
7AI(H_2O)$_2$	69	*1*	70	*8*	78		
7AI(H_2O)$_3$ bridged-planar	69	*4*	73	*6*	79	*11*	90
7AI(H_2O)$_3$ cyclic-nonplanar	77	*12*	91	*8*	99		
7AI(H_2O)$_3$ bicyclic-nonplanar	70	*35*	105	*10*	115		
7AI(H_2O)$_4$	74	*9*	83	*12*	95		
7AI(H_2O)$_5$	74	*11*	85	*26*	111		

To test the performance of the SVP-SV(P) basis set, the energy of points along a trajectory was recomputed with ADC(2)/TZVPP. The results show only minor differences between the two levels (<3 kcal.mol^{-1}) in the excited-state energy profile (see Figure 2.6).

1) 7AI(H_2O)$_3$ cluster

1.1) Bridged-planar isomer

From 50 trajectories starting at the bridged-planar isomer, three trajectories showed 7AI tautomerization within 300 fs through a quadruple PT process (Table 2.2). Triple ESPT after HBR occurred in only one trajectory, but in later times as discussed below. Tautomerization did not occur in 46 trajectories during the simulation time. Back PT reaction was observed in 1 trajectory.

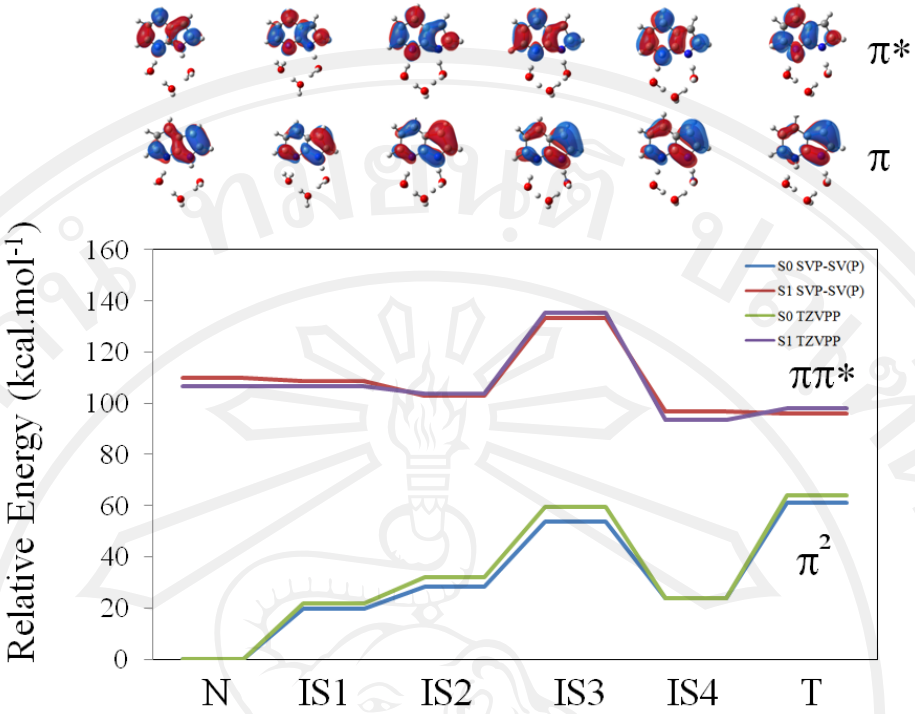

Figure 2.6 Comparison of relative single-point energies at RI-ADC(2)/SVP-SV(P) and RI-ADC(2)/TZVPP of the ground and first excited states (S_0 and $\pi\pi^*$) of a selected trajectory for the 7AI$(H_2O)_3$-bridged-planar cluster

The structures along the proton-transfer pathway are shown in Figure 2.7, and average values of forming bonds, breaking bonds, and energies for the three trajectories following the quadruple ESPT reaction are shown in Figure 2.8. The PT process, represented by arrows in Figure 2.7, can be visualized as the following sequence of events (atom labels are given in Figure 2.3a): a normal (N) form is observed at time 0. The first proton (H1) moves from the pyrrole ring to O1 atom of the nearest water (PT1) at 69 fs (when N1··H1 and O1··H1 bond distances are equal to 1.29 A° see Figure 2.8a) and right after that a proton is transferred from this water to the second water (PT2) at 73 fs (O1··H2 and O3··H2 equal to 1.30 A °). The third proton is transferred from the second water to the third water (PT3) at 79 fs (O2··H3 and O3··H3 equal to 1.31 A°). Afterward, the forth proton moves from the third water to N2 in the pyridine ring (PT4) at 90 fs (O2··H4 and N2··H4 equal to 1.33 A°). After completing the reaction, the cluster separates. This dynamic behavior is a sequence of synchronous PT processes. In the first 100 fs, the relative energy difference of S_1-S_0 (Figure 2.8b) gradually decreases. After the tautomerization is completed, the energy gap is still around 46 kcal.mol^{-1}, reflecting the planarity of the 7AI skeleton during the simulation time.

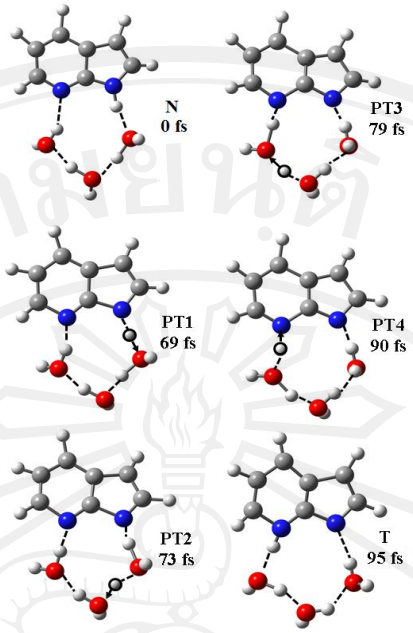

Figure 2.7 Snapshots of the 7AI$(H_2O)_3$-bridged-planar dynamics showing the time evolution of the ESQPT reaction through the hydrogen-bonded network. Normal (N), proton transfer (PT), and tautomer (T). Values correspond to the average over all ESQPT trajectories

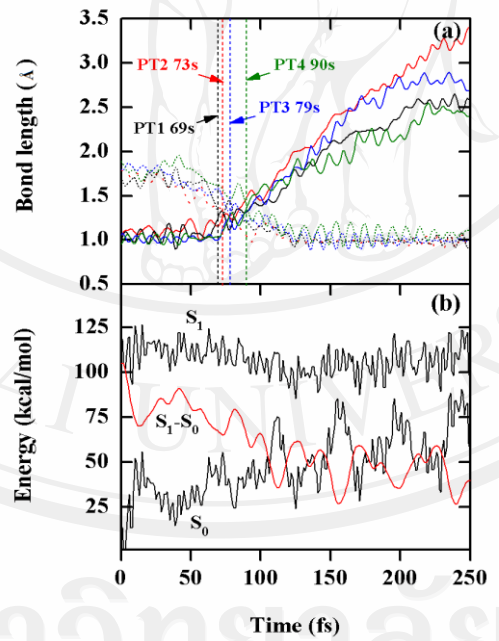

Figure 2.8 Average values over quadruple ESPT trajectories of the 7AI$(H_2O)_3$-bridged-planar isomer. (a) Average breaking and forming of bonds showing time evolution. N1–H1 and O1··H1 in black, O1–H2 and O3··H2 in red, O3–H3 and O2··H3 in blue, and O2–H4 and N2··H4 in green. (b) Average relative energies of excited state (S_1), ground state (S_0), and energy difference between S_1 and S_0 state (S_1-S_0)

A subset of five trajectories that ended without tautomerization was extended until 1,000 fs. One of these trajectories exhibited HBR leading the bridged-planar to cyclic-nonplanar isomer. After HBR, triple PT was initiated. Snapshots of this trajectory are shown in Figure 2.9. This pathway has been previously proposed by Yu et al. [73]. Considering that the small tautomerization probability for this isomer in the short timescale and the occurrence of HBR in one of the extended trajectories, we may speculate that this rearrangement may be a relevant pathway. Nevertheless, simulation of a larger number of trajectories in the long timescale would be needed to provide a quantitative estimate of its importance.

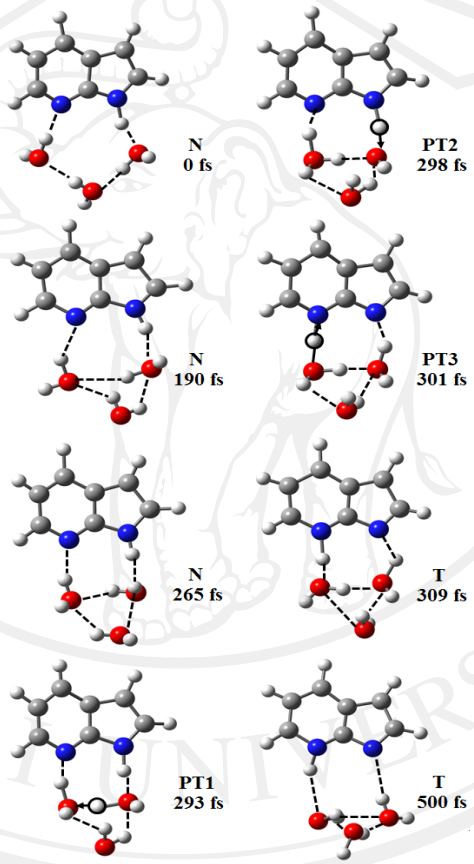

Figure 2.9 Snapshots of one trajectory of the 7AI$(H_2O)_3$-bridged-planar dynamics showing the HBR in waters leading it to form 7AI$(H_2O)_3$-cycylic-nonplanar isomer following by triple PT at 500 fs. Normal (N), Proton transfer (PT), and Tautomer (T)

1.2) Cyclic-nonplanar isomer

7AI tautomerization through triple ESPT reaction took place in 19 out of 50 trajectories (38 % probability, Table 2.2), while no proton transfer reaction was observed in 31 trajectories. Back PT reaction was also observed in 11 trajectories.

Snapshots illustrating the triple ESPT are displayed in Figure 2.10, and the atom numbering scheme given in Figure 2.3b is used to describe the dynamics. The values of the forming and breaking bonds averaged over all ESPT trajectories are given in Table 2.2 (see also Figure 2.11). Starting from the normal form (N) at time 0, the PT process is summarized in the following steps: first, the first proton (H1) departs from N1 to O1 (PT1) at 77 fs (N1··H1=O1··H1 at 1.30 A°), and then, the second proton (H2) of the first water moves from O1 to O2 (PT2) at 91 fs (O1··H2=O2··H2 at 1.34 A°). Finally, the third proton (H3) leaves the second water to the N2 in pyridine ring (PT3) at 99 fs (N1··H1=O1··H1 at 1.35 A°). Tautomerization is complete in 105 fs and it is followed by dissociation of the cluster.

There are 14 fs time lag between the first and the second PT and 8 fs between the second and the third PT. This indicates two synchronous processes. As in the previous cluster, the S_1-S_0 energy gap gradually decreases in the first 100 fs. After that, the average energy difference is always slightly below 50 kcal.mol^{-1}, and no intersection between the two states is approached within the simulation time.

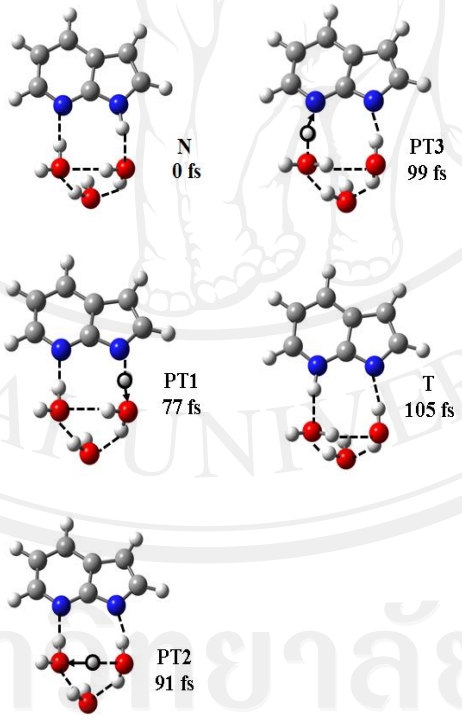

Figure 2.10 Snapshots of the 7AI(H_2O)$_3$-cyclic-nonplanar dynamics showing the time evolution of the triple ESPT reaction through the hydrogen-bonded network. Normal (N), proton transfer (PT), and tautomer (T). Values correspond to the average over all triple ESPT trajectories

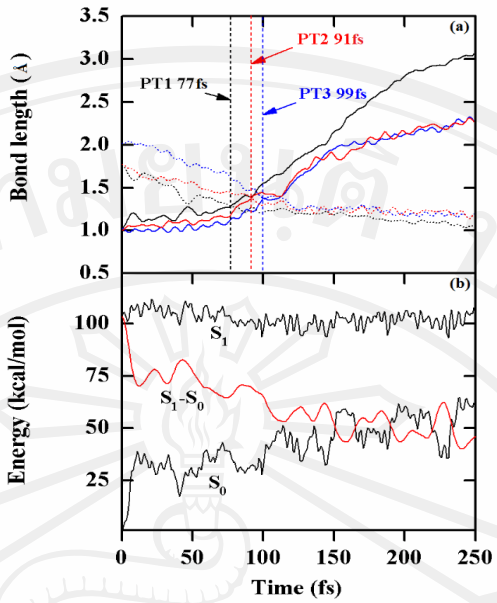

Figure 2.11 Average values over 19 trajectories of the 7AI$(H_2O)_3$ cyclic-nonplanar (2+1) isomer. (a) Average breaking and forming of bonds showing time evolution. N1–H1 and O1··H1 in black, O1–H2 and O2··H2 in red, and O2–H3 and N2··H3 in blue (b) Average relative energies of excited state (S_1), ground state (S_0), and energy difference of S_1 and S_0 state (S_1-S_0)

1.3) Bicyclic-nonplanar isomer

Thirty trajectories exhibited 7AI tautomerization through triple ESPT reaction (60 %, Table 2.2), 16 though O2 and 14 though O3 (see numbering in Figure 2.3c). Twenty trajectories showed no tautomerization within the simulation time. Back PT reaction was also observed in 6 trajectories.

Tautomerization in this cluster can occur through two symmetry-equivalent pathways, above and below the 7AI plane. Snapshots of a trajectory are depicted in Figure 2.12. The first PT takes place at 70 fs (N1–H1=O1–H1=1.27 A°, Table 2.2). The second PT occurs at 105 fs for a 1.34 A° O–H distance. The third PT takes place at 115 fs for a 1.35 A° O–H distance (Figure 2.13).

There is a 35 fs time lag between the first and second PT and 10 fs time lag between the second and third PT. The relatively long time delay between the first and the second PT can be attributed to a competition between O2 and O3 to receive the proton. H2 and H4 are pulled back and forth toward O2 and O4, respectively, few times before the transfer actually happens. This behavior implies that the triple proton transfer correspond to a concerted process followed by synchronous process.

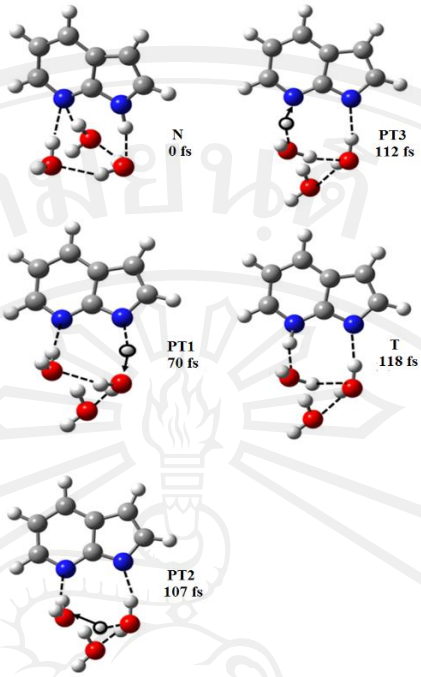

Figure 2.12 Snapshots of the 7AI$(H_2O)_3$-bicyclic-nonplanar dynamics showing the time evolution of the triple ESPT reaction through the hydrogen-bonded network. Normal (N), proton transfer (PT), and tautomer (T). Values correspond to the average over all triple ESPT trajectories

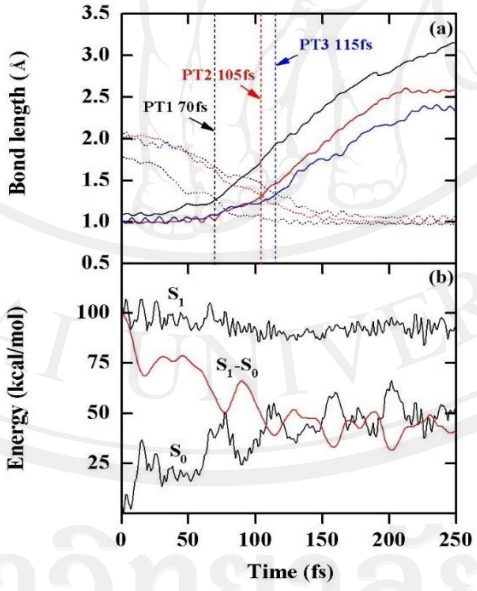

Figure 2.13 Average values over 30 trajectories of the 7AI$(H_2O)_3$ bicyclic-nonplanar isomer. (a) Average breaking and forming of bonds showing time evolution. N1–H1 and O1··H1 in black, O1–H2 and O2··H2 in red, and O2–H3 and N2··H3 in blue (b) Average relative energies of excited state (S_1), ground state (S_0), and energy difference of S_1 and S_0 state (S_1-S_0)

2) 7AI(H_2O)$_4$ cluster

Tautomerization via circuit1 (Figure 2.4a) occurred in 41 out of 50 trajectories (82 %, Table 2.2). It did not take place in nine trajectories during the simulation time. One trajectory exhibited quintuple ESPT reaction through four waters (circuit2). Back PT reaction was also observed in 17 trajectories.

The structures along the reaction pathway are shown in Figure 2.14. From our results averaged over the ESPT trajectories (see Figure 2.15), the times for PT1 (N1··H1=O1··H1 at 1.27 A°), PT2 (O1··H2=O2··H2 at 1.31 A°), and PT3 (O2··H3=N2··H3 at 1.29 A°) are 74, 83 and 95 fs, respectively. Time lags of 9 fs (between the PT1 and PT2) and 12 fs (between the PT2 and PT3) were observed, corresponding to two synchronous processes.

For the single trajectory with quintuple ESPT reaction via circuit2, the following events took place: proton transfers from N1 of pyrrole to the first water (O1), then to the second water (O3), then to the third water (O4), then to the forth water (O2) and finally to N2 of pyridine. The transfer times were 64, 78, 90, 95, and 104 fs, respectively.

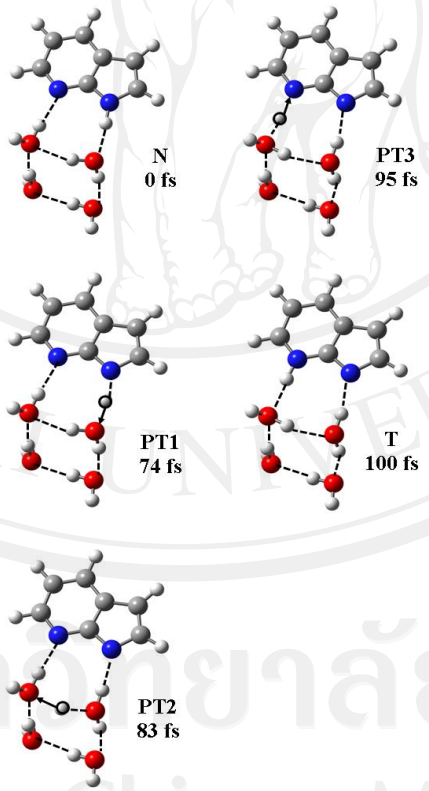

Figure 2.14 Snapshots of the 7AI(H_2O)$_4$ dynamics showing the time evolution of the triple ESPT reaction through the hydrogen-bonded network. Normal (N), proton transfer (PT), and tautomer (T). Values correspond to the average over all triple ESPT trajectories

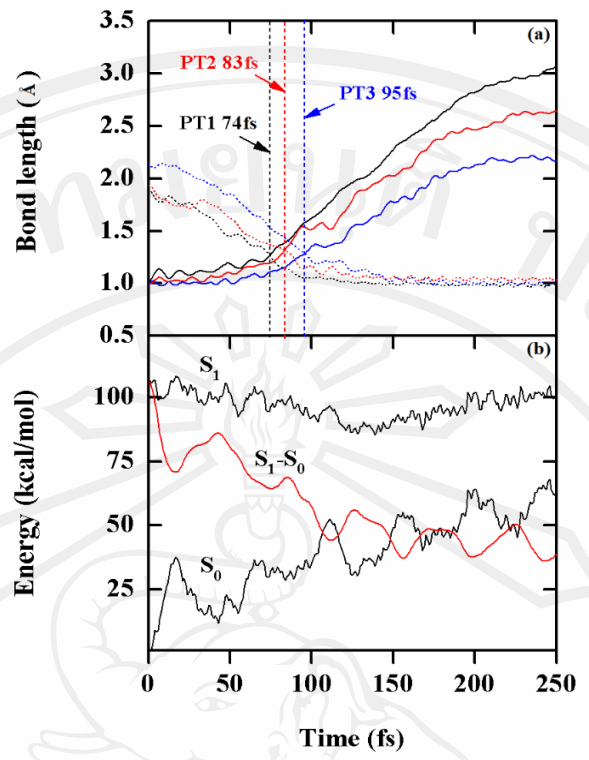

Figure 2.15 Average values over 40 trajectories of the 7AI$(H_2O)_4$. (a) Average breaking and forming of bonds showing time evolution. N1–H1 and O1··H1 in black, O1–H2 and O2··H2 in red, and O2–H3 and N2··H3 in blue (b) Average relative energies of excited state (S_1), ground state (S_0), and energy difference of S_1 and S_0 state (S_1-S_0)

3) 7AI$(H_2O)_5$ cluster

From 50 trajectories, 41 trajectories (82 %, Table 2.2) showed 7AI tautomerization through circuit1 and circuit2 (see Figure 2.4b), while no reaction was observed in 9 trajectories within the simulation time. Thirty-eight trajectories showed triple ESPT reaction through two waters (circuit1), whereas only three trajectories exhibited the sextuple ESPT reaction through five waters (circuit2). Back PT reaction was also observed in 18 trajectories.

Details of the triple ESPT process are depicted in Figure 2.16 and Table 2.2 (see also Figure 2.17). Transfer times for PT1 (N1··H1=O1··H1 at 1.27 A°), PT2 (O1··H2=O2··H2 at 1.33 A°), and PT3 (O2··H3=N2··H3 at 1.27 A°), averaged over ESPT trajectories, are 74, 85, and 111 fs, respectively. Time lags of 11 fs (between the PT1 and PT2) and 26 fs (between the PT2 and PT3) were observed, corresponding to a synchronous process followed by a concerted process.

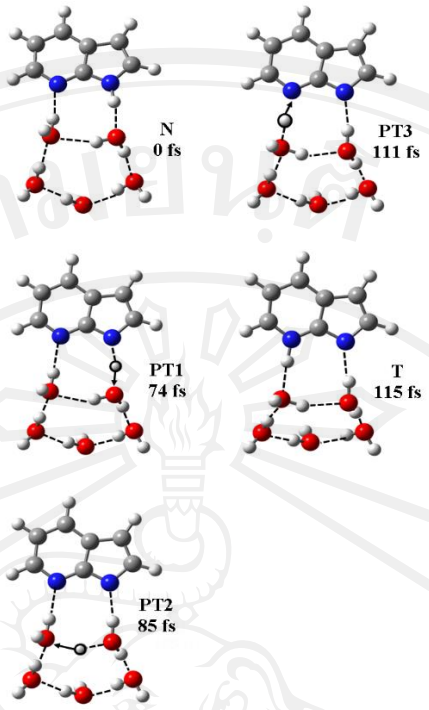

Figure 2.16 Snapshots of the 7AI$(H_2O)_5$ dynamics showing the time evolution of the triple ESPT reaction through the hydrogen-bonded network. Normal (N), proton transfer (PT), and tautomer (T). Values correspond to the average over all triple ESPT trajectories

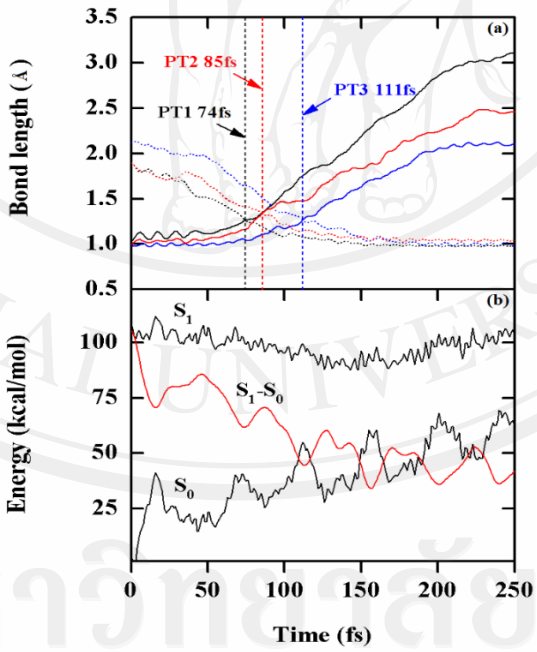

Figure 2.17 Average values over 38 trajectories of the 7AI$(H_2O)_5$. (a) Average breaking and forming of bonds showing time evolution. N1–H1 and O1··H1 in black, O1–H2 and O2··H2 in red, and O2–H3 and N2··H3 in blue (b) Average relative energies of excited state (S_1), ground state (S_0), and energy difference of S_1 and S_0 state (S_1-S_0)

4) 7AI(H_2O)$_1$, 7AI(H_2O)$_{1+1}$, and 7AI(H_2O)$_2$ clusters

The main aim of this work is to investigate the effect of the second hydration shell on the ultrafast ESPT. Nevertheless, for a matter of completeness, we have simulated the dynamics of clusters with one and two water molecules as well. The main results are reported in Tables 2.2, 2.4 and Figure 2.18b.

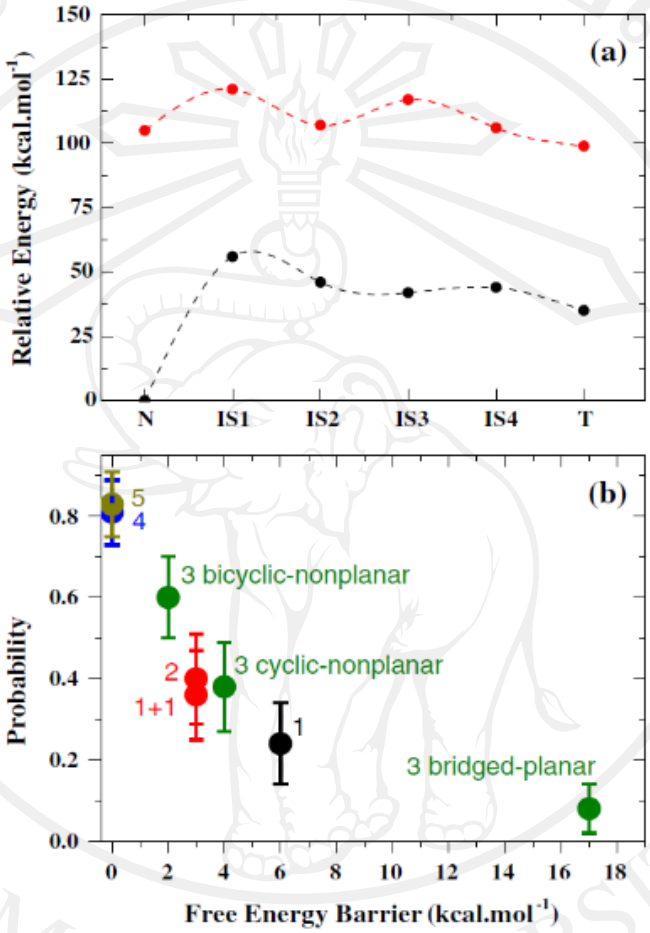

Figure 2.18 (a) Average relative energies of the ground (S_0) and the first excited states ($\pi\pi^*$) of 7AI(H_2O)$_3$-bridged-planar isomer. (b) Tautomerization probability versus free energy barrier for all clusters. The labels aside each symbol indicate the number of water molecules and the isomer

For 7AI(H_2O)$_1$, tautomerization occurs through a double PT with 24 % probability. It is completed in less than 100 fs (see Figures 2.19 and 2.20).

With two waters, we investigated the dynamics starting from two isomers: a 7AI(H_2O)$_{1+1}$ isomer, where a single water makes the bridge for double PT, while the second water is in the second shell; and a 7AI(H_2O)$_2$ isomer, where the two waters form a bridge allowing tautomerization via triple PT.

Table 2.4 Tautomerization probabilities and free energy barriers for ESPT reactions in the excited state computed from the dynamics simulations

Initial isomer	Tautomerization Probability	Barrier ($kcal.mol^{-1}$)	ESPT
$7AI(H_2O)_1$	0.24 ± 0.10	6	D
$7AI(H_2O)_{1+1}$	0.36 ± 0.11	3	D
$7AI(H_2O)_2$	0.40 ± 0.11	3	T
$7AI(H_2O)_3$-bridged-planar	0.06 ± 0.06	17	Q
$7AI(H_2O)_3$-cyclic-nonplanar	0.38 ± 0.11	4	T
$7AI(H_2O)_3$-bicyclic-nonplanar	0.60 ± 0.10	2	T
$7AI(H_2O)_4$	0.82 ± 0.08	0	T
$7AI(H_2O)_5$	0.82 ± 0.08	0	T

D double, *T* triple, *Q* quadruple

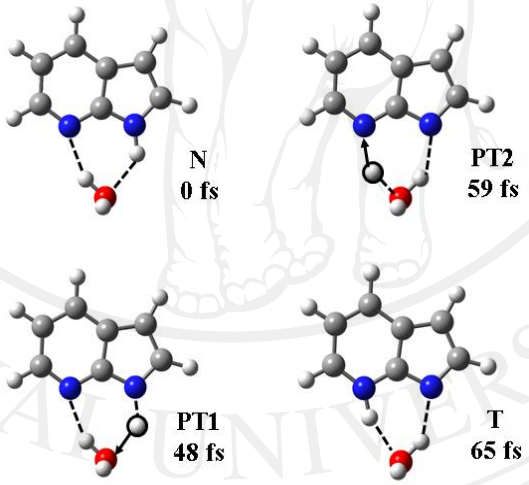

Figure 2.19 Snapshots representing the average over 12 trajectories of the $7AI(H_2O)_1$ showing the time evolution of the ESTPT reaction through a hydrogen-bonded network within 83 fs. Normal (N), proton transfer (PT), and tautomer (T)

Dynamics starting from the $7AI(H_2O)_{1+1}$ isomer is very similar to the single-water case. Tautomerization occurs through double PT in less than 100 fs. Tautomerization probability, however, tends to increase due to the network stabilization caused by the external water. More details about the dynamics results are given in Figures 2.21 and 2.22.

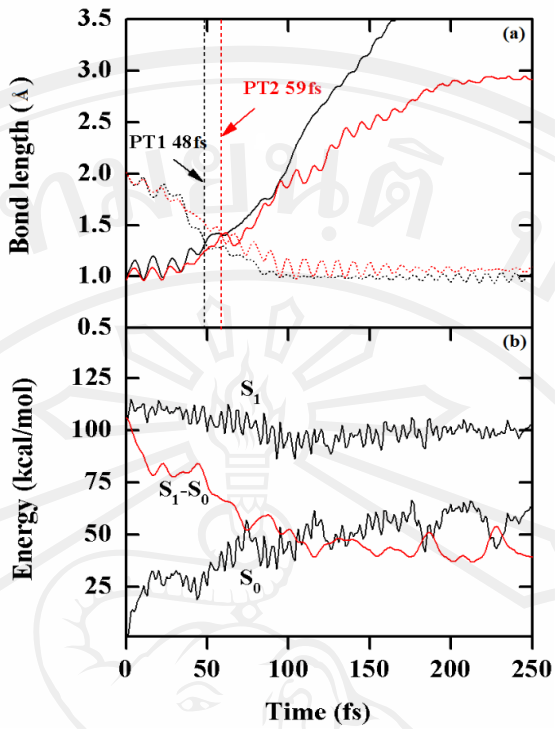

Figure 2.20 Average values over 12 trajectories of the 7AI(H_2O)$_1$. (a) Average breaking and forming of bonds showing time evolution. N1–H1 and O1··H1 in black, and O1–H2 and N2··H2 in red (b) Average relative energies of excited state (S_1), ground state (S_0), and energy difference of S_1 and S_0 state (S_1-S_0)

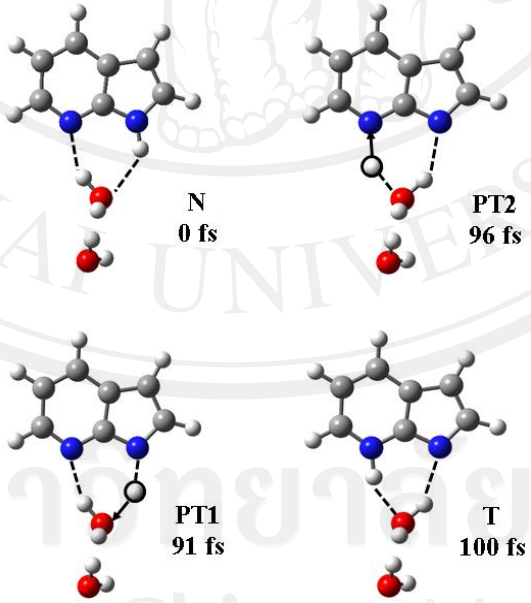

Figure 2.21 Snapshots representing the average over 18 trajectories of the 7AI(H_2O)$_{1+1}$ showing the time evolution of the ESTPT reaction through a hydrogen-bonded network within 83 fs. Normal (N), proton transfer (PT), and tautomer (T)

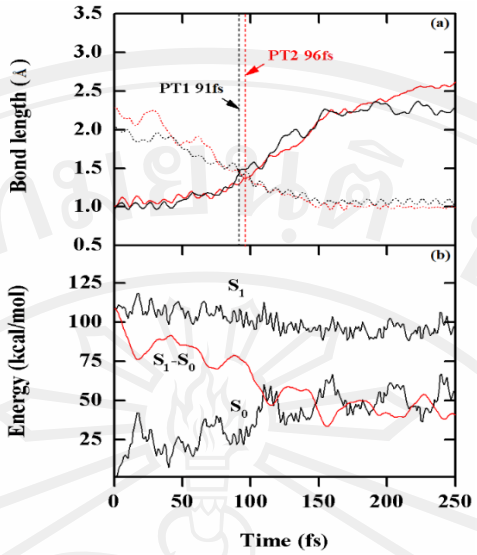

Figure 2.22 Average values over 18 trajectories of the 7AI$(H_2O)_{1+1}$. (a) Average breaking and forming of bonds showing time evolution. N1–H1 and O1··H1 in black, and O1–H2 and N2··H2 in red (b) Average relative energies of excited state (S_1), ground state (S_0), and energy difference of S_1 and S_0 state (S_1-S_0)

In Ref. [47], we discussed the dynamics of 7AI$(H_2O)_2$ in the context of the effect of water–methanol mixing. In the present work, we extended the number of simulated trajectories from 25 to 50, but the results remain, as expected, essentially the same. Tautomerization occurs through triple PT with 40 % probability. It is also completed within 100 fs. More details are given in Figures 2.23 and 2.24.

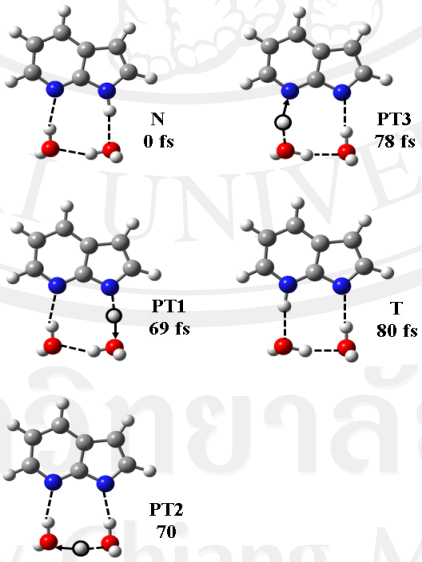

Figure 2.23 Snapshots representing the average over 20 trajectories of the 7AI$(H_2O)_2$ showing the time evolution of the ESTPT reaction through a hydrogen-bonded network within 83 fs. Normal (N), proton transfer (PT), and tautomer (T)

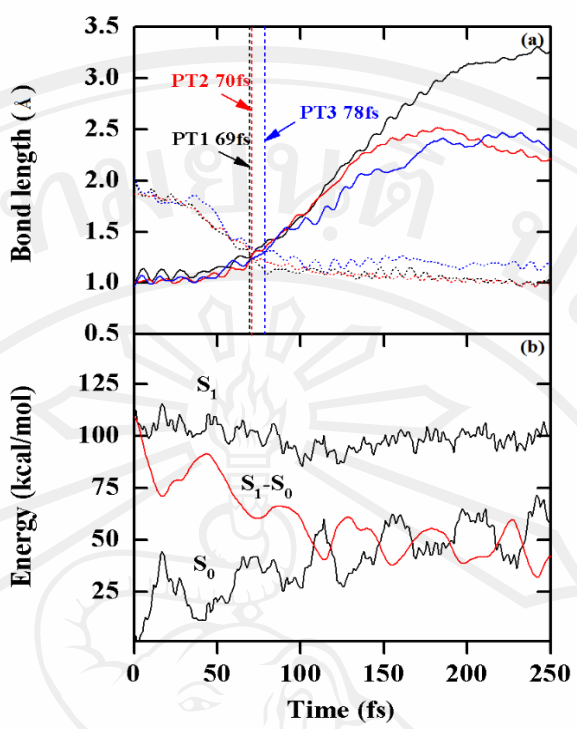

Figure 2.24 Average values over 20 trajectories of the 7AI$(H_2O)_2$. (a) Average breaking and forming of bonds showing time evolution. N1–H1 and O1··H1 in black, O1–H2 and O2··H2 in red, and O2–H3 and N2··H3 in blue (b) Average relative energies of excited state (S_1), ground state (S_0), and energy difference of S_1 and S_0 state (S_1-S_0)

2.3.3 Comparative analysis

For each cluster, energies of the ground (S_0) and first excited ($\pi\pi^*$) states averaged over all ESPT trajectories were computed along the reaction pathway for the following structures: initial tautomer (N), intermediary structure for each PT (IS_n), and final tautomer (T). These average energies for the 7AI$(H_2O)_3$-bridged-planar isomer are shown in Figure 2.18a. For the other clusters, they are plotted in Figure 2.25-2.31. For each cluster, the highest average energy barrier is given in Table 2.4. The barriers computed in this way are, in fact, an approximation to the free energy barrier obtained by thermodynamic integration of independent trajectories [90] following Gaussian reaction paths. They are in good agreement with relative energies computed on the first excited singlet electronic state using TD-B3LYP by Casadesus et al. [77]. A good agreement is also observed between the barrier for 7AI$(H_2O)_1$ computed here (6 kcal.mol^{-1}) and the zero-point-corrected energy barrier computed with multi-reference perturbation theory to second order (MRPT2) reported in Ref. [69] (6.39 kcal.mol^{-1}).

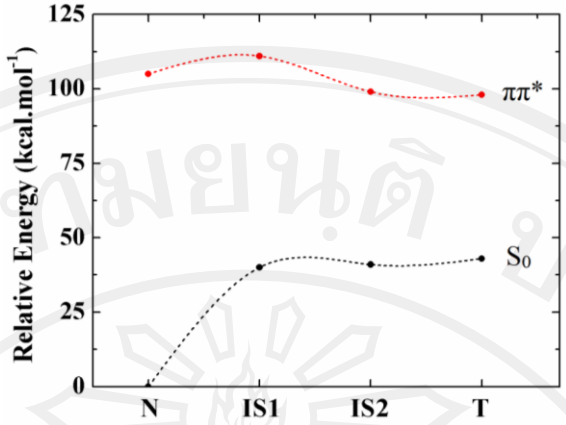

Figure 2.25 Average relative energies (kcal.mol^{-1}) of the ground (S_0) and the excited states ($\pi\pi^*$) of 7AI$(H_2O)_1$

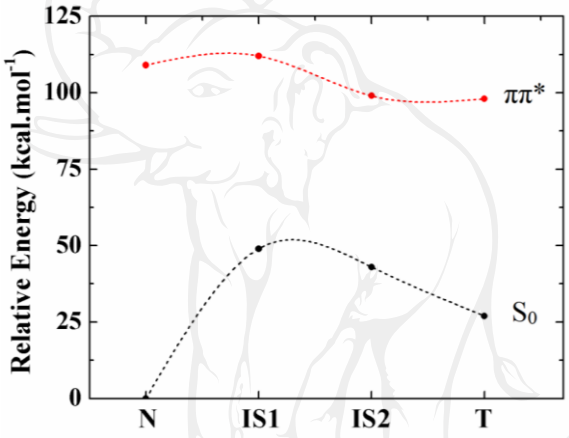

Figure 2.26 Average relative energies (kcal.mol^{-1}) of the ground (S_0) and the excited states ($\pi\pi^*$) of 7AI$(H_2O)_{1+1}$

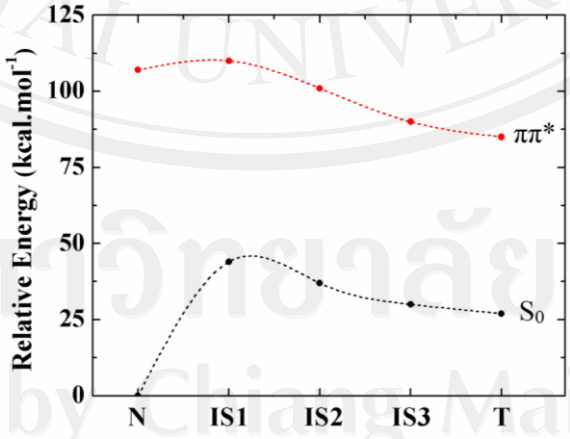

Figure 2.27 Average relative energies (kcal.mol^{-1}) of the ground (S_0) and the excited states ($\pi\pi^*$) of 7AI$(H_2O)_2$

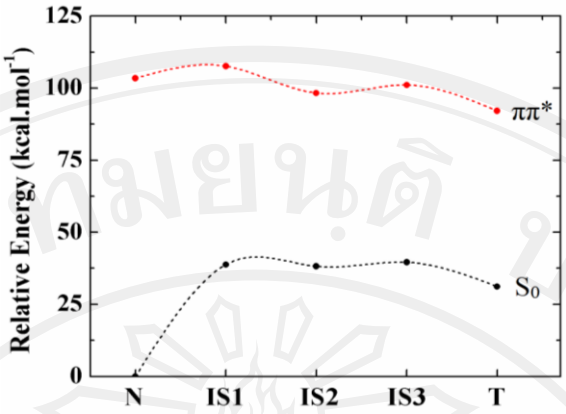

Figure 2.28 Average relative energies (kcal.mol^{-1}) of the ground (S_0) and the excited states ($\pi\pi^*$) of 7AI$(H_2O)_3$-cyclic-nonplanar (2+1) isomer

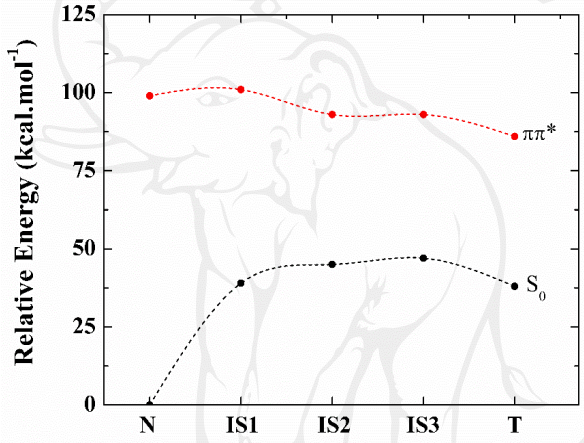

Figure 2.29 Average relative energies (kcal.mol^{-1}) of the ground (S_0) and the excited states ($\pi\pi^*$) of 7AI$(H_2O)_3$-bicyclic-nonplanar isomer

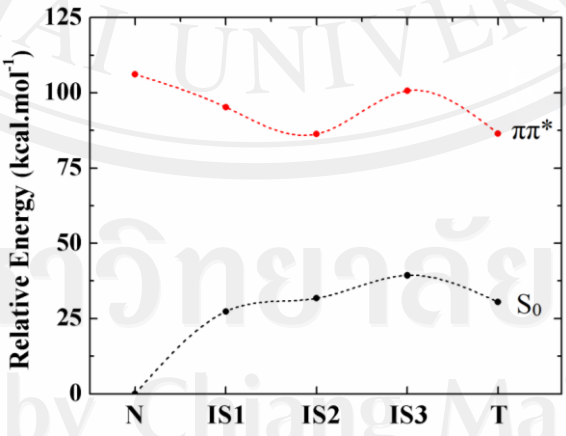

Figure 2.30 Average relative energies (kcal.mol^{-1}) of the ground (S_0) and the excited states ($\pi\pi^*$) of 7AI$(H_2O)_4$

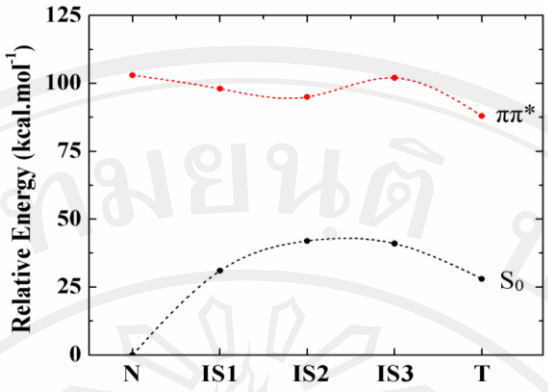

Figure 2.31 Average relative energies (kcal.mol^{-1}) of the ground (S_0) and the excited states ($\pi\pi^*$) of 7AI$(H_2O)_5$

The free energy barriers are nicely anti-correlated with the tautomerization probabilities (Table 2.4; Figure 2.18b): the case with largest barrier, 7AI$(H_2O)_3$-bridged-planar (17 kcal.mol^{-1}), has only 6 % probability, while the cases with the smallest barriers, 7AI$(H_2O)_4$ and 7AI$(H_2O)_5$ (0 kcal.mol^{-1}), have 82 % probability of tautomerization.

In the two cases where double ESPT occurs, 7AI$(H_2O)_1$ and 7AI$(H_2O)_{1+1}$, the addition of one external water to form the latter cluster cuts the barrier by half, increasing the tautomerization probability from 24 to 36 % (note, however, that these values are within the error bar for a 90 % confidence interval). In the cases where triple ESPT occurs, the clusters are arranged with 7AI$(H_2O)_{2+n}$ (n = 0–3) structure. As explained above, triple ESPT occurs through the two internal waters (circuit1), while the n other external waters remain as spectators, contributing to the overall stability of the hydrogen-bonded network. Once more, the increase in the number of waters in the second shell tends to reduce the barrier and increase the tautomerization probability. A saturation of this effect is observed already for n = 2 (4 waters), when the process becomes barrierless.

Most complexes share a common pattern: after photoexcitation, it takes about 70 fs to trigger the PT process (see Table 2.2). Exceptions are 7AI$(H_2O)_1$ and 7AI$(H_2O)_{1+1}$ which have the PT triggered in 48 and 91 fs, respectively. In all cases, as soon as the first PT is initiated, it facilitates a fast sequence of proton transfers through the bridge until the tautomerization is reached within about 100 fs. The PT times (Table 2.2) indicate that synchronous processes take place in 7AI$(H_2O)1$, 7AI$(H_2O)_{1+1}$, 7AI$(H_2O)_2$, 7AI$(H_2O)_3$-bridged-planar, 7AI$(H_2O)_3$-cyclic-nonplanar, and 7AI$(H_2O)_4$. A sequence of concerted then-synchronous-processes takes place in 7AI$(H_2O)_3$-bicyclic-nonplanar and a sequence of synchronous then concerted processes takes place in 7AI$(H_2O)_5$.

As discussed in the introduction, spectroscopic results at the S_1 band origin [68, 70] imply much longer PT times than those that we have described. The main reason for the difference is that in our simulations, the whole S_1 band is excited, providing enough energy to overcome the tautomerization barriers. We have also seen that the tautomerization probability is relatively small for clusters with up to three waters, meaning that even with this excess of energy, substantial fraction of the excited population should tautomerize in longer timescales.

2.4 Conclusions

On-the-fly molecular dynamics simulations in the first excited state (S_1) of $7AI(H_2O)_{1–5}$ clusters were carried out at RI-ADC(2)/SVP-SV(P) level. The following conclusions concerning the excited-state proton-transfer process and the effect of the second hydration shell on it can be drawn from our results:

- Multiple excited-state proton transfers through a hydrogen-bonded network are observed in the 100-fs scale.
- The probability of tautomerization is anti-correlated with the maximum free energy barrier in the excited state. The range of probability is between 8 and 82%.
- An increasing number of water molecules tends to reduce the barrier by strengthen the hydrogen-bonded network. Barrierless reactions are found already for clusters with four waters.
- In structures presenting double hydrogen bond circuits, proton transfer happens mostly through the internal circuit by triple proton transfer. Thus, the main role of the second hydration shell is of stabilizing the network, facilitating the proton transfer.
- Proton transfer occurs mostly in the original ground state conformation that the complex has at the time of photoexcitation. We found, however, qualitative evidence of sub-picosecond photoinduced hydrogen bond reorganization of $7AI(H_2O)_3$ from the bridged-planar to cyclic-nonplanar isomer prior the proton transfer.
- Although rare, quintuple, and sextuple proton transfers were observed. They are completed in about 100 fs.
- The proton transfer tends to be composed of synchronous steps, with two of them occurring within 10–15 fs apart.